AIP Journal of Applied Physics

Influence of thermal annealing on the electron emission of InAs quantum dots containing a misfit defect state

J. F. Chen, C. H. Yang, R. M. Hsu, and U. S. Wang

Citation: Journal of Applied Physics **105**, 063705 (2009); doi: 10.1063/1.3081654
View online: http://dx.doi.org/10.1063/1.3081654
View Table of Contents: http://scitation.aip.org/content/aip/journal/jap/105/6?ver=pdfcov
Published by the AIP Publishing

Articles you may be interested in
Presentation and experimental validation of a model for the effect of thermal annealing on the photoluminescence of self-assembled InAs/GaAs quantum dots
J. Appl. Phys. **107**, 123107 (2010); 10.1063/1.3431388

Annealing of self-assembled InAs/GaAs quantum dots: A stabilizing effect of beryllium doping
Appl. Phys. Lett. **94**, 072105 (2009); 10.1063/1.3086298

Effects of alloy intermixing on the lateral confinement potential in In As Ga As self-assembled quantum dots probed by intersublevel absorption spectroscopy
Appl. Phys. Lett. **90**, 163107 (2007); 10.1063/1.2724893

Effect of incorporating an InAlAs layer on electron emission in self-assembled InAs quantum dots
J. Appl. Phys. **99**, 014303 (2006); 10.1063/1.2150258

Widely tunable intersubband energy spacing of self-assembled InAs/GaAs quantum dots due to interface intermixing
J. Appl. Phys. **86**, 2687 (1999); 10.1063/1.371111

Re-register for Table of Content Alerts

Create a profile.

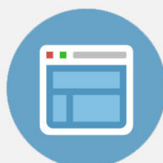

Sign up today!

[This article is copyrighted as indicated in the article. Reuse of AIP content is subject to the terms at: http://scitation.aip.org/termsconditions. Downloaded to] IP: 140.113.38.11 On: Wed, 30 Apr 2014 15:26:01

JOURNAL OF APPLIED PHYSICS 105, 063705 (2009)

Influence of thermal annealing on the electron emission of InAs quantum dots containing a misfit defect state

J. F. Chen,[a] C. H. Yang, R. M. Hsu, and U. S. Wang
Department of Electrophysics, National Chiao Tung University, Hsinchu, Taiwan 30050, Republic of China

(Received 9 October 2008; accepted 10 January 2009; published online 18 March 2009)

We have investigated the effect of postgrowth thermal annealing on the electron emission from InAs quantum dots (QDs) containing a misfit-related defect state induced by strain relaxation. Additional carrier depletion in the GaAs bottom layer near the QD, caused by the defect state, can effectively suppress electron tunneling from the QD, leading to the observation of a thermal emission from the QD electron ground state to the GaAs conduction band with a large emission energy of 213 meV, in contrast to defect-free nonrelaxed QDs in which an emission of 58 meV from the QD electron ground state to first excited state is observed. The emission energy is reduced to 193 meV and to 164 meV after annealing at 650 and 700 °C for 1 min, respectively. This emission energy reduction is correlated with the photoluminescence blueshift which is attributed to the interdiffusion of atoms across the QD interface. The electron emission from the QD first excited and ground states is found to be a thermal emission at high temperatures and a tunneling emission at low temperatures. The tunneling energy barrier is found to be comparable to the thermal emission energy, supporting a thermal emission to the GaAs conduction band. This study illustrates a significant effect of a defect state on the electron-emission process in the QDs, suggesting the possibility of modifying the electron emission time of the QDs by purposely introducing a deep defect state. © *2009 American Institute of Physics*. [DOI: 10.1063/1.3081654]

I. INTRODUCTION

Transitions between the conduction-band (CB) states of InAs self-assembled quantum dots (QDs) (Refs. 1–8) are in the long-wavelength infrared region and referred to as intraband transitions. Understanding the electron emission mechanism[9–12] is important for infrared applications such as photodetectors.[13,14] Kapteyn *et al.*[9] observed a two-step electron emission process: a thermal emission from the QD electron ground state (EGS) to first excited state (FES) and then tunneling to the GaAs CB, rather than a thermal emission from the QD EGS to the GaAs CB. This work and related studies[10,11] suggest a significant tunneling emission for the electrons escaping from the QDs. Lowering the background concentration in the GaAs barrier layer is expected to increase the tunneling width and suppress the tunneling emission. Another approach is to induce additional carrier depletion in the GaAs barrier layer by purposely introducing a deep defect state. Defect-free coherent QDs can be formed by partial strain relaxation. However, when InAs deposition thickness exceeds a critical thickness (~3 ML), strain is relaxed by inducing lattice misfits.[15,16] With an InGaAs strain-reducing capping layer,[17] the misfits are confined near the QD bottom interface and behave like electron-trapping centers. These deep levels can cause additional carrier depletion and suppress the tunneling emission, leading to a significant modification of the electron emission process in the QDs. Postgrowth thermal annealing[18–22] is expected to shift upward the QD electron states because a blueshift of photoluminescence (PL) is usually observed due to the interdiffusion of atoms across the QD interface. Thus, it would be interesting to study the effect of the thermal annealing on the electron emission from the QDs and compare the results with the PL spectra. In this work, the electron emission from relaxed InAs QDs, subjected to thermal annealing at different temperatures, are systematically investigated using capacitance-voltage (*C-V*) profiling and admittance spectroscopy. Due to the long emission time, the misfit-related defect state is probed by voltage-dependent deep-level-transient spectroscopy (DLTS).

II. EXPERIMENTS

The InAs QDs with an InGaAs capping layer were grown on n^+-GaAs (100) substrates by solid source molecular beam epitaxy in a Riber machine. On top of a 0.3-μm-thick Si-doped GaAs $[(6-10)\times 10^{16}\ \mathrm{cm}^{-3}]$ barrier layer, an InAs layer with different deposition thicknesses from 2 to 3.3 ML was deposited at 490 °C (at a rate of 0.26 Å/s) to form the QDs. The DLTS and cross-sectional transmission electron microscopy (TEM) detected no defects when the InAs deposition thickness is less than 3 ML. However, when the InAs deposition thickness exceeds 3 ML, lattice misfits and an associated deep level, along with a sudden PL blueshift, are observed,[23] indicative of strain relaxation in the QDs. Following the growth of the QD layer, a 60-Å $In_{0.15}Ga_{0.85}As$ capping layer and a 0.2-μm-thick Si-doped GaAs $[(6-10)\times 10^{16}\ \mathrm{cm}^{-3}]$ barrier layer were grown to terminate the growth. Detailed growth conditions can be found elsewhere.[24] A typical QD sheet density of about $3\times 10^{10}\ \mathrm{cm}^{-2}$ was observed by atomic force microscopy (AFM). Postgrowth annealing was performed by rapid thermal annealing. For *C-V* profiling, Schottky diodes were re-

[a]Electronic mail: jfchen@cc.nctu.edu.tw.

[This article is copyrighted as indicated in the article. Reuse of AIP content is subject to the terms at: http://scitation.aip.org/termsconditions. Downloaded to] IP: 140.113.38.11 On: Wed, 30 Apr 2014 15:26:01

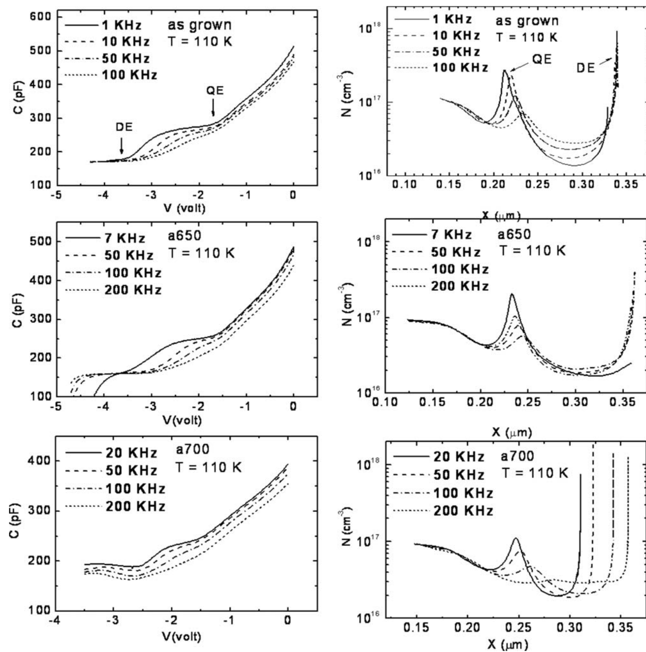

FIG. 1. *C-V* profiling and converted apparent carrier distributions at 110 K for relaxed QDs with InAs deposition thickness of 3.3 ML for the as-grown samples and samples annealed at 650 and 700 °C, respectively. Two capacitance plateaus with corresponding carrier peaks, denoted as QE and DE, can be seen. Strain relaxation induces a defect state which causes the DE emission and drastic carrier depletion on the bottom GaAs side.

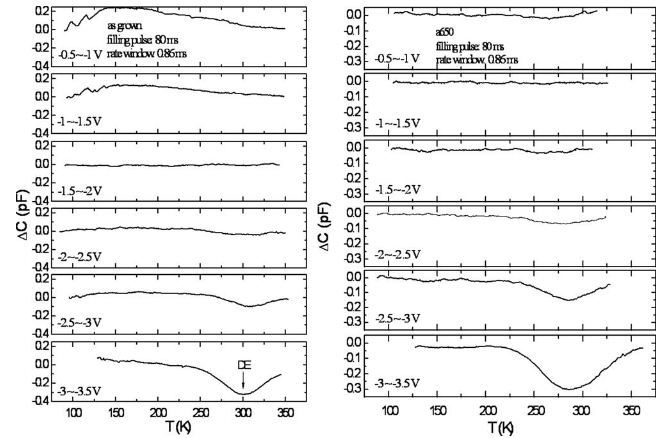

FIG. 2. DLTS spectra of the relaxed QDs as grown and annealed at 650 °C, measured at different quiescent voltages with a fixed sweeping step of 0.5 V. In both samples, no signals are observed in the top GaAs layer. For quiescent voltage of −3 V (−3 to −3.5 V), a trap signal can be seen at around ~300 K with activation energies of 0.38 and 0.36 eV for the as-grown QDs and QDs annealed at 650 °C, respectively. By comparison with the *C-V* profiling in Fig. 1, this trap corresponds to the DE peak.

alized by evaporating Al on sample surface. The *C-V* profiling and admittance spectroscopy were performed using HP 4194A impedance analyzer. PL measurements were carried out using a double frequency Nd-doped yttrium aluminum garnet laser at 532 nm.

III. MEASUREMENT AND RESULTS

A. Electron distribution in the QDs

To see the electron distribution in the QDs, Fig. 1 shows the *C-V* and converted carrier profiling (at 110 K) for as-grown relaxed InAs QDs with InAs deposition thickness of 3.3 ML and for QDs annealed at 650 °C (denoted as a650) and 700 °C (denoted as a700) for 1 min, respectively. Annealing does not much affect the profiling. Two distinct *C* plateaus starting at about −1.5 and −3.5 V, as denoted by quantum emission (QE) and defect emission (DE), can be seen. Significant leakage current starts to appear after −4 V. The QE plateau is converted to a carrier peak near the QD spatial position (0.2 μm). For the as-grown QDs, the peak is slightly asymmetric with a weak shoulder on the right side (at 0.23 μm). Prominent asymmetric shape was observed in defect-free nonrelaxed QDs in which the right shoulder was identified to be the electron emission from the QD EGS and the peak was identified to be the electron emission from the excited state (ES) of the QDs (to be shown). Note that for the three samples, the depletion on both sides of the QE peak is rather asymmetric. The valley concentration (for the as-grown QDs at 1 KHz) is 1.5×10^{16} cm^{-3} on the bottom GaAs side, which is much smaller than that of 5×10^{16} cm^{-3} on the front GaAs side, and the broadness of the depletion on the bottom GaAs side is more than double of that on the front GaAs side. This additional carrier depletion on the bottom GaAs side is attributed to the misfit-related defect state induced by strain relaxation in the QDs. This additional carrier depletion can significantly affect the electron emission from the QDs to the GaAs bottom layer. After the QE peak, when reverse voltage is further applied, Fermi level will eventually intersect with the misfit defect state, leading to the emergence of the DE plateau in the *C-V* profiling. The corresponding deep depth of 0.34 μm (for the as-grown QDs) cannot be interpreted as the spatial location of the defect state. The defect state is localized near the QD and neighboring GaAs bottom layer. Due to its being deeper in energy, when Fermi level crosses the defect state, the edge of the Schottky depletion region is already moved to a depth of about 0.34 μm. From a simple Schottky depletion model, a rough estimation from the spatial separation between the QE and DE peaks yields that the defect state is about 0.3 eV below the QE peak state. This energy position is consistent with that to be revealed by DLTS. The *C-V* profiling clearly indicates the presence of two electron emissions: one from a shallow QD state and the other from the deep state. Note that as ac frequency is increased, the intensity of the QE peak attenuates, suggesting a resolvable time constant. We will determine its emission time by admittance spectroscopy in Sec. III C. As to the DE peak, due to its long emission time, its time constant is revealed by DLTS.

B. DLTS characterization of the misfit defect state

Figure 2 shows the DLTS spectra for the as-grown QDs and a650. To evaluate the spatial location, the quiescent voltage is decreased with a sweeping step of 0.5 V. The filling pulse duration time is selected to be 80 ms to saturate the intensity of the defect state. Both samples show no signals until the quiescent voltage is decreased to about −3.5 V, corresponding to the starting voltage (−3.5 V) of the DE plateau in Fig. 1, and thus the observed trap (at ~300 K) shall correspond to the DE peak. The Arrhenius plots yield

[This article is copyrighted as indicated in the article. Reuse of AIP content is subject to the terms at: http://scitation.aip.org/termsconditions. Downloaded to] IP: 140.113.38.11 On: Wed, 30 Apr 2014 15:26:01

activation energies (capture cross sections) of 0.38 eV (1.42×10^{-16} cm^2) and 0.36 eV (8.1×10^{-17} cm^2) for the as-grown QDs and a650, respectively. The DLTS spectra reveal no signal related to the QE peak due to its too short emission time. Further decreasing the quiescent voltage beyond −4 V, a rapid increasing leakage current renders the DLTS measurements very difficult. The parameter of this DE trap is similar to that (0.395 eV, 1×10^{-16} cm^2) observed by Uchida *et al.*[16] in strain relaxed InGaAs/GaAs quantum well structures. This defect state is associated with relaxation-induced lattice misfits observed by Fourier transformed cross-sectional TEM.[25] Annealing at 650 °C does not much affect the concentration and emission parameters of this defect state. We had investigated the DLTS spectra by varying filling pulse duration time and found that the amplitude of the defect state saturated when filling pulse duration time was increased to about 1 ms. The feature of saturation suggests an isolated point defectlike nature for the misfit defect state. The saturated peak intensity of $\Delta C=0.3$ pF in Fig. 2 yields a sheet density of about 4.1×10^9 cm^{-2} from $N_T=N_D(\Delta C/C_0^2)\varepsilon A$, where $N_D=1\times10^{17}$ cm^{-3}, $C_0=200$ pF, area $A=5\times10^{-3}$ cm^2, and permittivity $\varepsilon=1.14\times10^{-10}$ F/m. This density is approximately one order of magnitude less than the QD sheet density (about 3×10^{10} cm^{-2} from AFM), and thus the concentration of the defect state is not large enough to cause a complete depletion of the electrons in the QDs. This can explain the observation of the QE peak, consistent with the PL spectra which clearly show the QD ground and first excited transitions at 300 K (to be shown).

C. Electron emission from the QDs

We can roughly estimate the density of the electrons accumulated in the QDs by evaluating the underlying area of the QE peak in Fig. 1. From the lowest ac frequency as indicated, we obtain sheet densities of 2.78×10^{11}, 2.69×10^{11}, and 2.06×10^{11} cm^{-2} for the as-grown QDs and a650 and a700, respectively. Annealing seems to slightly reduce the concentration of the electrons in the QDs. A comparison with the QD density of $\sim3\times10^{10}$ cm^{-2} suggests that the electrons fill up to the FES of the QD. The frequency-dependent attenuation of the QE peak allows us to determine the emission time by measuring the conductance as a function of frequency and temperature at the dc voltages corresponding to the QE plateau in Fig. 1 (−2 to −3.4 V for the as-grown QDs, −1.3 to −3.2 V for a650, and −1.5 to −2.6 V for a700). Figure 3 shows the conductance/frequency-frequency (G/F-F) spectra at a dc voltage corresponding to the near ending of the QE plateau (the electrons in the QDs are nearly emptied) for the as-grown QDS and a650 and a700, respectively. The oscillation level is selected as 10 mV. For each temperature, the G/F curve displays a peak at a frequency corresponding to emission rate. As shown in Fig. 3, for a same temperature, the peak is shifted to a higher frequency after annealing, suggesting that annealing can reduce the emission time. Figure 4 shows the Arrhenius and logarithmic plots of the emission time (the inverse of the emission rate) as a function of dc voltage. From the logarithmic plots, the emission time displays a strong temperature dependence at a high temperature and a near temperature independence at a low temperature. Thus, electron emission from the QDs transits from a thermal emission to a tunneling emission when temperature is lowered. From the Arrhenius plots at high temperatures, the thermal emission energy are obtained to be 91–213 meV from −2 to −3.4 V for the as-grown QDs, 86–193 meV from −1.6 to −3.2 V for a650, and 52–164 meV from −1.6 to −2.6 V for a700. Table I summarizes the bias-dependent emission energies and capture cross sections for the three samples.

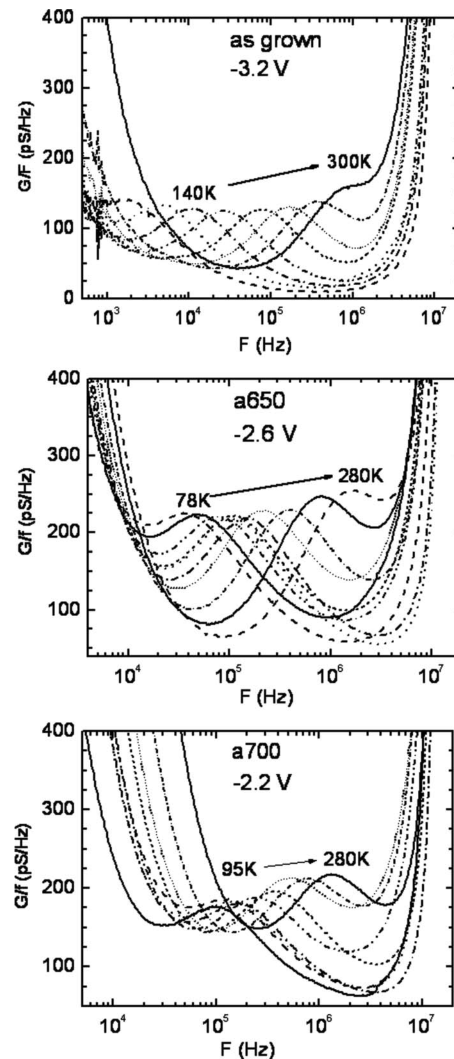

FIG. 3. The G/F-F spectra measured on the QE peaks for the as-grown relaxed InAs QDs and those annealed at 650 and 700 °C, respectively. The dc voltages correspond to the near emptying of the QD electron GS.

The bias-dependent emission energy for the electron emission from the QDs is not due to an electric field effect because increasing the amplitude of the electric field would decrease, not increase, the emission energy. This observation suggests a bandlike electron state for the QDs. As estimated from the area of the QE peak, the QE peak shall consist of the QD EGS and FES. Thus, the observed energy from 91 to 213 meV for the as-grown QDs may represent the two states and the 213 meV is the highest bound of the EGS. As shown in Fig. 1, the QE peak for the as-grown QDs is asymmetric

[This article is copyrighted as indicated in the article. Reuse of AIP content is subject to the terms at: http://scitation.aip.org/termsconditions. Downloaded to] IP: 140.113.38.11 On: Wed, 30 Apr 2014 15:26:01

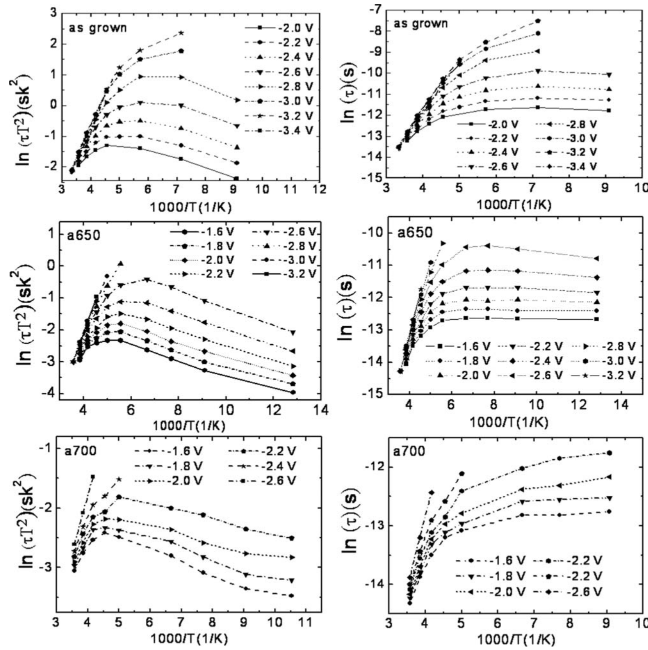

FIG. 4. Arrhenius and logarithmic plots of the electron emission times in the relaxed QDs as grown and annealed at 650 and 700 °C, respectively. The strong temperature dependence at high temperatures suggests a thermal emission. The near temperature independence at low temperatures suggests a tunneling emission.

with a right shoulder. When temperature is lowered below 100 K, the QE peak starts to split into two peaks, as shown in Fig. 5. Since Fermi level first crosses the higher energy state when reverse dc voltage is applied, the peaks at 0.25 and 0.28 μm shall be the QD FES (denoted as ES) and the EGS [denoted as GS (for ground state)], respectively. Let us try to distinguish the spectral ranges of the two states. In Fig. 5(a), the indicated voltage of −2.25 V represents the dc voltage for the near emptying of the electrons of the FES and starting to deplete the EGS and the voltage of −3.4 V represents the emptying of the EGS. Thus, we use the corresponding emission energy of 119 meV for −2.25 V to separate the two states. As a result, the energy from 91 to 119 meV is considered as the FES and the energy from 119 to 213 meV as the

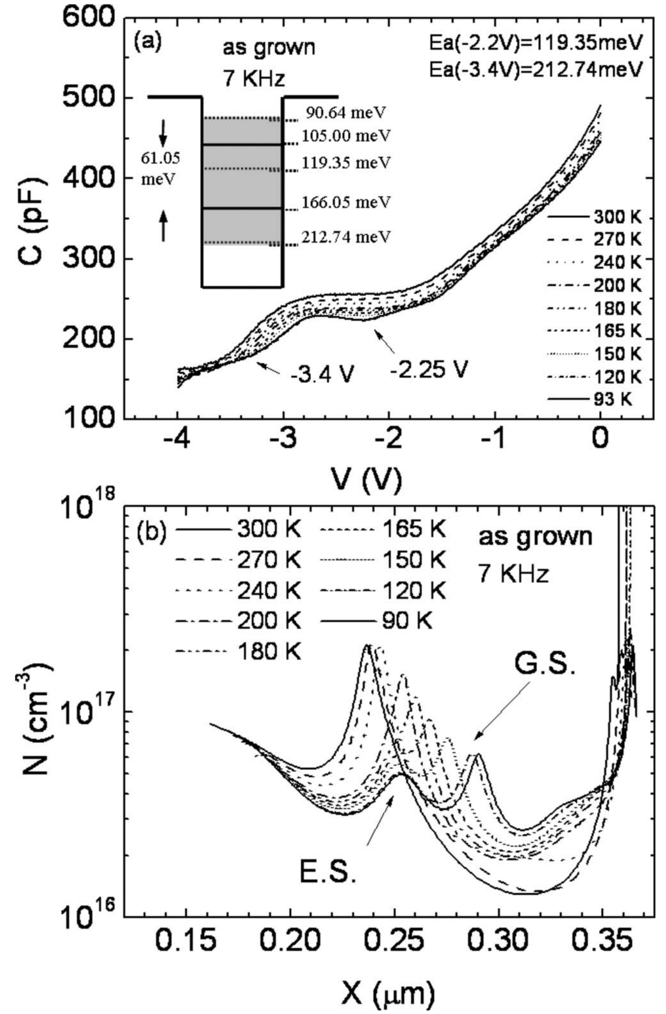

FIG. 5. (a) Temperature-dependent *C-V* profiling and corresponding (b) carrier distributions of the as-grown relaxed InAs QDs. When temperature is below 100 K, the QE plateau is split into two plateaus corresponding to the QD FES and the GS. The dc voltage of −2.25 V represents the near emptying of the FES and the beginning depopulation of the GS. Its corresponding emission energy of 119 meV is used to distinguish the two states. The averaged GS and FES are separated by 61 meV.

TABLE I. Electron thermal emission energies and capture cross sections of the QDs, measured at different dc biases for the as-grown samples and samples annealed at 650 and 700 °C.

3.3 ML, as grown			3.3 ML, annealed at 650 °C			3.3 ML, annealed at 700 °C		
Bias (V)	E_a (meV)	Capture cross section (cm^2)	Bias (V)	E_a (meV)	Capture cross section (cm^2)	Bias (V)	E_a (meV)	Capture cross section (cm^2)
−2	90.64	1.97×10^{-20}	−1.3	86.3	2.81×10^{-18}	−1.5	51.67	2.91×10^{-19}
−2.2	119.35	4.09×10^{-18}	−1.4	92.77	3.66×10^{-18}	−1.7	70.42	1.56×10^{-18}
−2.4	144.03	1.03×10^{-17}	−1.6	109.87	1.11×10^{-17}	−1.8	87.45	3.15×10^{-18}
−2.6	169.47	2.64×10^{-17}	−1.8	122.61	1.87×10^{-17}	−2.0	91.60	3.51×10^{-18}
−2.8	191.56	6.18×10^{-17}	−2.2	122.61	1.48×10^{-17}	−2.2	95.53	3.72×10^{-18}
−3.0	200.27	8.11×10^{-17}	−2.4	148.10	4.29×10^{-17}	−2.4	112.78	7.02×10^{-18}
−3.2	201.88	8.75×10^{-17}	−2.6	161.21	7.00×10^{-17}	−2.6	164.30	5.36×10^{-17}
−3.4	212.74	1.96×10^{-16}	−2.8	171.22	1.02×10^{-16}			
			−3.0	184.92	1.84×10^{-16}			
			−3.2	192.71	2.78×10^{-16}			

[This article is copyrighted as indicated in the article. Reuse of AIP content is subject to the terms at: http://scitation.aip.org/termsconditions. Downloaded to] IP: 140.113.38.11 On: Wed, 30 Apr 2014 15:26:01

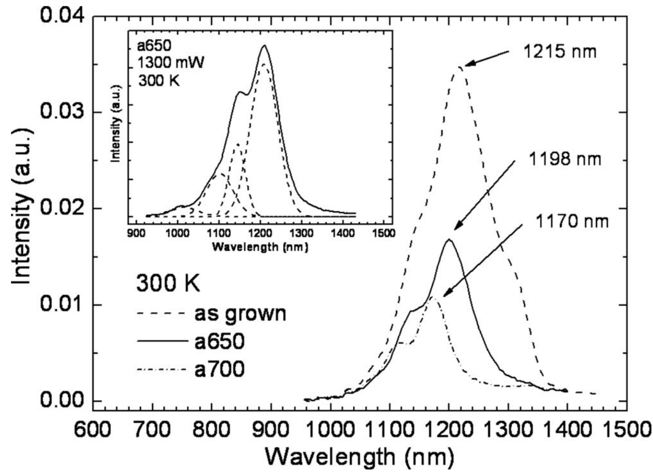

FIG. 6. 300-K PL spectra of relaxed InAs QDs for the as-grown QDs and samples annealed at 650 and 700 °C, respectively. Transitions from the QD GS and FES can be clearly seen. Blueshifts of 15 and 39 meV can be seen after annealing at 650 and 700 °C, respectively. The inset shows the fitting of the spectra of the annealing at 650 °C by three Gaussians corresponding to the ground, first excited, and second excited transitions.

EGS, yielding spectral broadness of 28 and 94 meV for the FES and EGS, respectively. By taking the averaged value as the energy position, assuming the emission energy is relative to the GaAs CB, the FES and EGS are 105 and 166 meV, respectively, below the GaAs CB, as shown in Fig. 5(a). These confinement energies are close to 96 and 190 meV reported by Kapteyn *et al.*,[9] and 60 and 140 meV reported by Brunkov *et al.*[26] for similar InAs QDs. This comparability supports the assignment of the QE peak as electron emission from the QDs, rather than from some defect states.

As aforementioned, the misfit defect state is about 0.3 eV below the QE peak state. If we take the FES (105 meV) as the peak state, the misfit defect state would be at about 0.4 eV below the GaAs CB, which is close to the activation energy (0.38 eV) of the trap observed by the DLTS. This consistency confirms that the defect state is localized near the QDs and the observed emission is relative to the GaAs CB. In order to confirm whether the electronic band structure in Fig. 5(a) is related to the FES and EGS of the QDs, we compare it with PL spectra. Figure 6 shows the 300-K PL spectra of the as-grown QDs, a650, and a700, respectively, under the excitation of 3.3 mW. Except for the spectrum for the as-grown QDs, which displays an additional peak at 1307 nm, each spectrum displays the ground (as indicated by 1215, 1198, and 1170 nm, respectively) and first excited transitions of the QDs. The peak at 1307 nm for the as-grown QDs is considered as a transition from another group of the QDs. In order to show this, Fig. 7(a) illustrates the temperature dependence of the as-grown QDS under an excitation power of 10 mW. When temperature is lowered, the ground (1215 nm) and the first excited (1150 nm) transitions significantly increase in intensity accompanied by a blueshift of about 50 meV (from 300 to 50 K), which is comparable to that observed in nonrelaxed QDs. In comparison, the intensity of the transition at 1307 nm only slightly increases, suggesting that the related group of the QDs are much smaller in number and are nearly filled up with carriers at 300 K, relative to the group of the QDs that give the 1215-nm transition. Increasing excitation power can lead to the emergence of the second excited transition of the QD group that gives the 1215-nm ground transition, as shown in the 300-K PL spectra in Fig. 7(b). The spectra are normalized by the ground transition at 1215 nm to illustrate the relative intensity

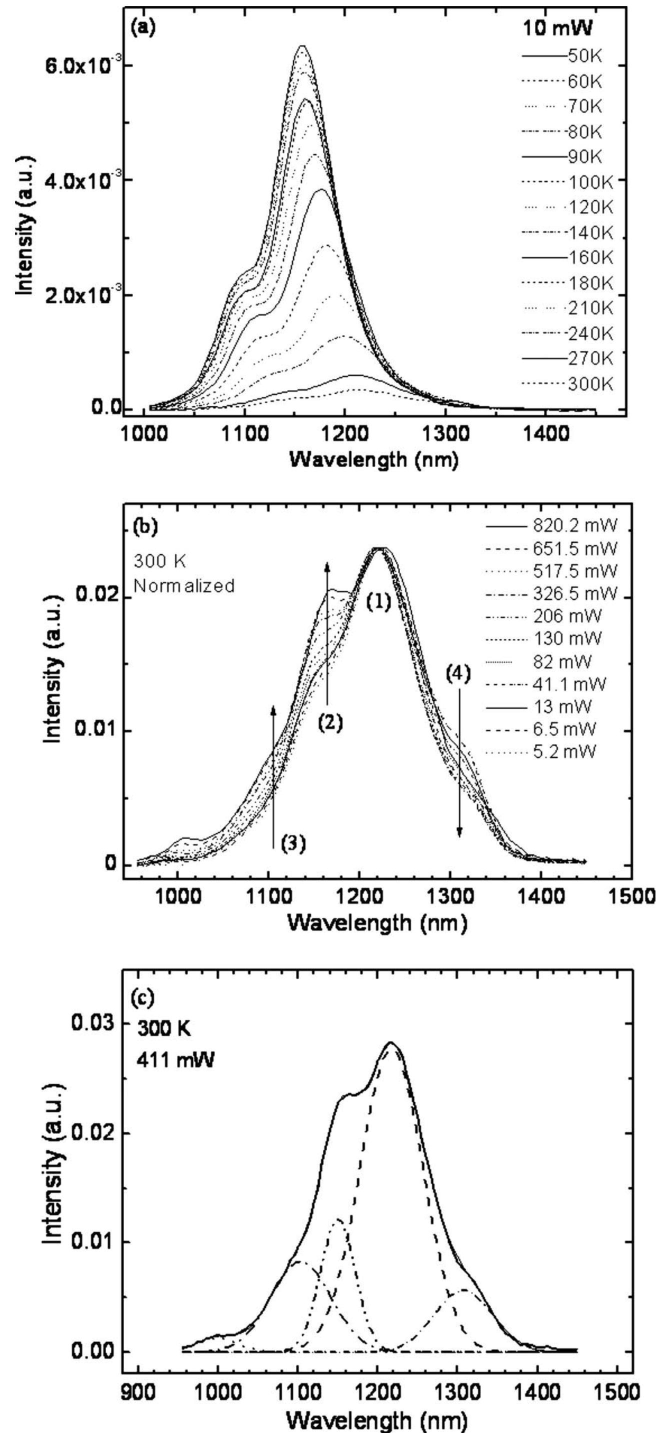

FIG. 7. (a) Temperature-dependent PL spectra of the as-grown QDs under an excitation power of 10 mW, illustrating a ground transition at 1215 nm and a first excited transition at 1150 nm. (b) Power-dependent PL spectra at 300 K. In order to show the relative intensity change, the spectra are normalized by the ground transition [denoted by (1)]. As excitation power increases, the first excited [denoted by (2)] and second excited [denoted by (3)] transitions are enhanced with respect to the ground transition. (c) The deconvolution of the 300-K PL spectra.

[This article is copyrighted as indicated in the article. Reuse of AIP content is subject to the terms at: http://scitation.aip.org/termsconditions. Downloaded to] IP: 140.113.38.11 On: Wed, 30 Apr 2014 15:26:01

TABLE II. Ranges of electron thermal emission energies of the QDs and the FWHMs of the PL GS and first excited state (ES) transitions for the as-grown samples and samples annealed at 650 and 700 °C.

	As grown	a650	a700
C-F	90.6 (ES)–212.7 (GS)	86.3 (ES)–192.7 (GS)	51.7 (ES)–164.3 (GS
(E_a)	□E=122.1 meV	□E=106.4 meV	□E=112.6 meV
PL	68.2 (GS) and 41.1 (ES)	77.3 (GS) and 30.0 (ES)	67.2 (GS) and 30.6 (ES)
(FWHM)	□E=109.3 meV	□E=107.3 meV	□E=97.8 meV

change. As power increases, in contrast to the transition at 1307 nm, the first excited [indicated by (2)] and second excited [indicated by (3)] transitions are enhanced with respect to the ground transition. This feature reflects limited filling of the GS and the filling of the ES by additional photogenerated carriers. Thus, transitions (1)–(3) should belong to the same group of the QDs. Increasing power does not appreciably enhance the 1307-nm transition, reflecting the fact that the related QDs are very low in number and are already filled up with carriers at low powers. From the deconvoluted 300-K spectra [Fig. 7(c)], the energy separations between the ground and first excited transitions and between the first and second excited transitions for the predominant group of the QDs are obtained as 59 and 45 meV, respectively, which are close to those observed in nonrelaxed QDs. Thus, the 1215-nm transition is considered as the ground transition of the predominant group of the QDs.

The detailed nature of the transition at 1307 nm is not fully understood. However, it is suspected to be a transition from some QDs that remain nonrelaxed. Note that its wavelength is close to the achievable longest wavelength before the onset of strain relaxation. When the InAs deposition thickness is below a critical relaxation thickness of 3 ML, increasing the InAs deposition thickness can redshift the ground transition to about a maximum of 1310 nm (at 300 K). When the InAs deposition thickness exceeds 3 ML, the ground transition undergoes a sudden blueshift of about 70 meV due to strain relaxation. Further increasing the InAs deposition thickness can further increase the blueshift. The longest wavelength achievable before strain relaxation is about 1300 nm. Thus, we suspect that at the onset of strain relaxation, due to size dispersion, a few QDs whose size is still below the critical size (with equivalent wavelength of 1300 nm) are probably not relaxed and give rise to the 1307-nm transition. Further increasing the InAs deposition thickness would enhance the degree of strain relaxation and reduce the numbers of these nonrelaxed QDs, which can explain the experimentally observed decreasing intensity of this transition. Figure 6 shows that the 1307-nm transition becomes invisible after annealing, suggesting that annealing probably can probably provide thermal energy for these remaining nonrelaxed QDs to relax and to blueshift its transition. In view of the above discussions, the nonrelaxed QDs are very few in number. Electron emission from these nonrelaxed QDs is expected to be very weak and fast, and thus electron emission from them is not considered. In fact, as shown in Fig. 5(b), the carrier distribution at 90 K exhibits a very weak bump at 0.33 μm. This bump is seen after the GS of the relaxed QDs, consistent with its relative long PL wavelength. Thus, this bump is likely related to the 1307-nm transition.

As shown in Fig. 6, the ground transition is blueshifted from 1.0206 to 1.0351 eV and further to 1.0598 eV after annealing at 650 and 700 °C, respectively. This blueshift is usually explained by the interdiffusion of atoms across the QD interface. The observation of these transitions suggests that the QD sates are not severely degraded by strain relaxation. Thus the electron emission from the related electron states is expected to be observed. We fit each spectrum by three Gaussians corresponding to the ground, first excited, and second excited transitions, as shown in the inset of Fig. 6 for a650. Table II shows the obtained full widths at half maximum (FWHMs) of the ground and first excited PL transitions (denoted as GS and ES) for the as-grown QDs and a650 and a700, respectively. For the as-grown QDs, the FWHMs are 68 and 41 meV for the ground and first excited transitions, which are close to 94 and 28 meV for the broadness of the QD EGS and FES shown in Fig. 5(a). The PL spectra show energy separation of 59 meV between the ground and first excited transitions, which is closed to that of 61 meV between the EGS and FES in Fig. 5(a). This comparability suggests a very small energy separation between the hole GS and FES, as previously claimed.[26] As shown in Table II, the total FWHM of the ground and first excited transitions for a650 is 107 meV, which is close to the whole range of 106 meV (from 86 to 193 meV) observed from the electron-emission energy from the QDs (*C-F* spectra). Similar closeness is observed for a700. This comparison shows comparable broadness and separation of the electron energy states and the corresponding PL transitions, supporting that the QE peak is originated from the QD EGS and FES.

Annealing can decrease the electron-emission energies of the QDs. For example, the highest-bound emission energy of the EGS decreases from 213 to 193 meV and to 164 meV after annealing at 650 and 700 °C, respectively. This implies upward energy shifts of 20 and 49 meV, which are close to the 300-K PL blueshifts of 15 meV (from 1.0206 to 1.0351 eV) and 39 meV (from 1.0206 to 1.0598 eV) as shown in Fig. 6. Thus, the reducing emission energy of the QD states can be correlated to the PL blueshift which is attributed to the interdiffusion of atoms across the QD interface. This result suggests that most of the energy shift induced by annealing is in the CB, consistent with the result of a theoretical calculation.[27] The consistency of the energy shift further supports the assignment of the QE peak as electron emission from the QDs, rather than from the misfit defect state to the QD state as previously suspected.[17] Since if it were, the up-

[This article is copyrighted as indicated in the article. Reuse of AIP content is subject to the terms at: http://scitation.aip.org/termsconditions. Downloaded to] IP: 140.113.38.11 On: Wed, 30 Apr 2014 15:26:01

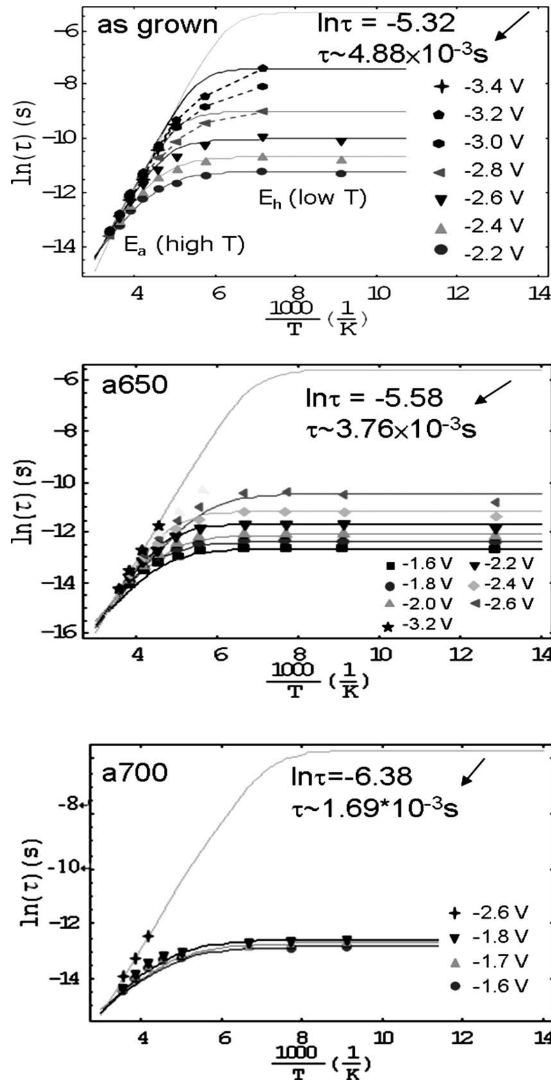

FIG. 8. Logarithmic plots of the electron emission times in the relaxed QDs for the as grown, annealing at 650 and 700 °C, respectively. These emission times can be well fitted by a combination of a thermal emission and a tunneling emission with the thermal emission barrier as the tunneling barrier.

ward shift of the QD state by annealing as implied by the PL blueshift would increase the emission energy, rather than decrease as experimentally observed. Hence, the QE peak is proved to be an electron emission from the QDs.

D. Electron emission mechanism from the relaxed QD

The logarithmic plots of the emission times in Fig. 4 suggest a combination of a thermal emission and a tunneling emission as expressed by the equation $e_n = e_{th} + e_{tun}$.[28] Here $e_{th} = \gamma T^2 \sigma_n \exp(-E_a/kT)$ is the thermal emission rate where $\gamma = 2.28 \times 10^{20}$ cm^{-2} s^{-1} K^{-2} for n-type GaAs, E_a is the thermal emission barrier and σ_n is the capture cross section, and $e_{tun} = (qF/4\sqrt{2m^* E_h})\exp[-(4/3)(\sqrt{2m^* E_h^3}/q\hbar F)]$ is the tunneling emission rate, where F is the electric field and E_h is the tunneling barrier height. From the Arrhenius plots at high temperatures, values of E_a and σ_n have been determined as listed in Table I. Values of the tunneling barrier height E_h can be fitted by the emission times at low temperatures in Fig. 4. We found that the fitted E_h is very close to E_a. This is illustrated in Fig. 8, in which the experimental data points can be fitted by the above theoretical expression (solid curves) using $E_h = E_a$. To further illustrate this point, Fig. 9 shows the experimental tunneling times (observed at low temperatures) for the as-grown QDs and a650 and a700 follow the theoretical tunneling time expression $\tau_{tun} = 1/e_{tun}$ with E_a as E_h. The fact that the thermal emission barrier is the tunneling barrier indicates that at high temperatures, electrons are thermally emitted from the QD states to the GaAs CB. This electron emission process is quite different from that observed in defect-free nonrelaxed QDs.[9,17]

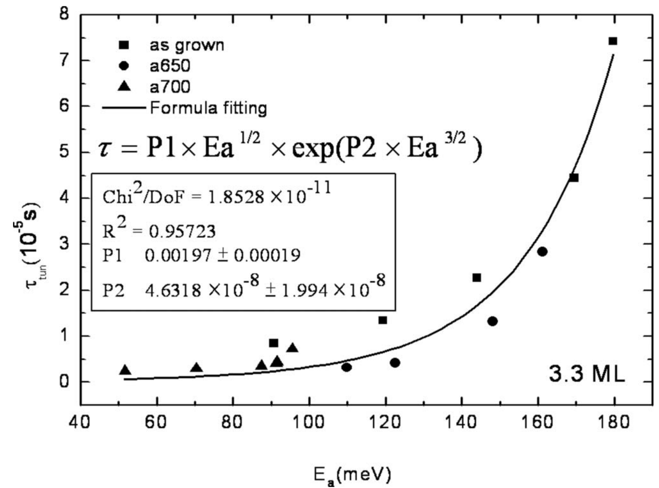

FIG. 9. The experimental tunneling times vs the thermal emission energies for the as-grown QDs and QDs after annealing at 650 and 700 °C, respectively. These data points follow the theoretical tunneling expression with the thermal emission barrier as the tunneling barrier.

E. Comparison with defect-free nonrelaxed QDs

For comparison, Fig. 10 shows 80-K C-V profiling and converted electron distribution for a nonrelaxed InAs QDs (capping with an InGaAs layer) with InAs deposition thick-

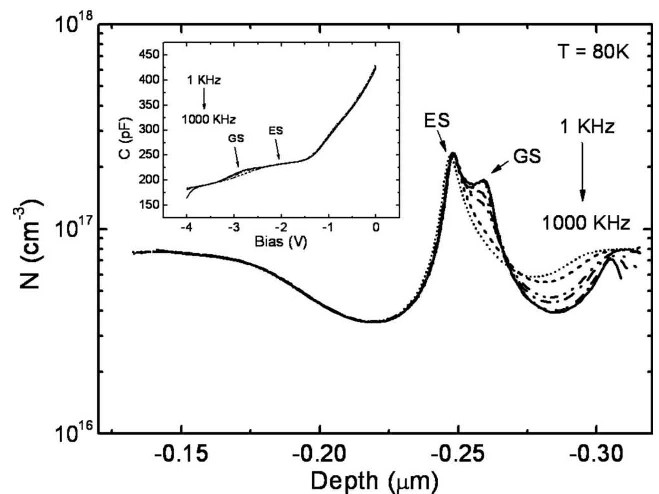

FIG. 10. Electron distribution and corresponding C-V profiling (in the inset) for nonrelaxed InAs QDs with InAs deposition thickness of 2.4 ML. One carrier peak at 0.25 μm with a shoulder at 0.26 μm is seen. The ES peak is attributed to the electrons tunneling from the QD ESs to the GaAs CB. The GS shoulder is attributed to a thermal excitation from the QD ground to FES and subsequently tunnels to the GaAs CB.

[This article is copyrighted as indicated in the article. Reuse of AIP content is subject to the terms at: http://scitation.aip.org/termsconditions. Downloaded to] IP: 140.113.38.11 On: Wed, 30 Apr 2014 15:26:01

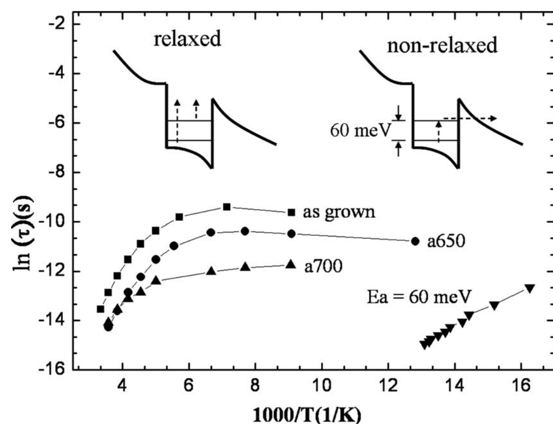

FIG. 11. Logarithmic plots of the electron emission times of the QD EGSs for the nonrelaxed InAs QDs (with emission energy of 60 meV), and relaxed InAs QDs as grown and annealed at 650 and 700 °C, respectively. CB schematic diagrams illustrate the emission processes for the nonrelaxed and relaxed InAs QDs.

ness of 2.4 ML. Electron emission from the QDs results in a capacitance plateau (−1.5 to −3 V) and its corresponding carrier peak at 0.25 μm (denoted as ES) with a clear shoulder bump at 0.26 μm (denoted as GS). Besides this plateau, no further plateau, such as the DE plateau observed in the relaxed QDs, is seen. Furthermore, the carrier depletion is rather symmetric on both sides of the peak. The ES peak is attributed to electrons in the QD ESs tunneling[9–11] to the GaAs CB. The emission time of this peak is too short to be resolved up to 1 MHz at 10 K. The GS shoulder shows frequency-dependent attenuation with an emission time on the order of 10^{-6} s (at 70 K) and with emission energy of ~60 meV,[17] as indicated in Fig. 11. This emission energy is comparable to the PL energy spacing between the ground and first excited transitions, and thus the shoulder bump is attributed to a thermal excitation from the QD EGS to FES and subsequently tunnels to the GaAs CB, in a two-stage emission process previously described,[9] as illustrated by a CB schematic diagram (nonrelaxed) in Fig. 11. The two-step emission mechanism for nonrelaxed QDs was previously corroborated by capping the InAs QDs with an InAlAs layer to increase the energy spacing between the EGS and FES and a comparable increase in this energy spacing and in the energy spacing between the PL ground and first excited transitions was ovserved.[29] Detailed discussions on the emission process in nonrelaxed QDs can be found elsewhere.[9,14]

When the InAs deposition thickness exceeds 3 ML, strain relaxation in the QDs occurs, accompanied with a sudden PL blueshift of about 70 meV in the ground transition[18] and the generation of a misfit defect state near the QD if the QD is capped with an InGaAs layer. Without the InGaAs capping layer, strain relaxation would generate additional threading dislocations in the top GaAs barrier layer.[30] Hence, the InGaAs capping layer can effectively relieve the strain in the top GaAs layer, leading to the occurrence of strain relaxation near the QD bottom interface. With the InGaAs capping layer, strain relaxation does not deplete much the carriers in the QDs. However, the induced misfit defect state can cause additional carrier depletion on the GaAs bottom side and suppress the tunneling emission from the QDs. As a result, electrons escaping out of the EGS and FES occur through a thermal emission to the GaAs CB (at high temperatures), as illustrated in the schematic diagram (relaxed) in Fig. 11, in which the detailed CB protrusion due to the additional carrier depletion is not shown. Highest-bound thermal emission energy of 213 meV is observed for the QD EGS for the as-grown QDs, with respect to 60 meV in the nonrelaxed QDs. Figure 11 shows that strain relaxation significantly elongates the emission time of the QD EGS. Annealing at 650 °C can reduce the highest-bound emission energy of the EGS to 193 meV and further to 164 meV after annealing at 700 °C. Figure 11 shows the emission times of the EGS for dc biases corresponding to the peak of the EGS. At low temperatures, inevitable tunneling emission appears. The tunneling times for the FES are on the order of 10^{-6} s, relative to an irresolvable short time in the nonrelaxed QDs. Since annealing does not much affect the concentration and emission parameters of the misfit defect state as implied by the DLTS, the decrease in the emission time and energy by annealing cannot be explained by the effect of the defect state. Judging from a comparable energy blueshift in the PL transition, the decrease in the emission time is attributed to an upward energy shift of the QD electron states due to interdiffusion of atoms across the QD interface. The results of the present studies illustrate a significant effect of a defect state on the electron-emission process in the QDs, offering the possibility of modifying the electron emission time of the QDs by purposely introducing a deep defect state.

IV. CONCLUSIONS

Electron distribution and emission in strain relaxed InAs QDs subjected to thermal annealing are investigated. Strain relaxation can introduce additional capacitance plateau due to the generation of a misfit defect state, leading to additional carrier depletion in the GaAs bottom side. This carrier depletion can suppress the tunneling emission from the QDs and change the electron emission process. Without the defect state, electrons escape from the GS through a thermal emission to the FES and then tunneling to the GaAs bottom layer. With the defect state, at high temperatures, electrons escape from the GS and FES via a thermal emission to the GaAs CB, leading to a significant increase in the emission time and energy. Annealing can reduce the emission time and energy due to an upward energy shift of the QD electron states, as evident from the observation of a similar energy shift in the PL transitions of the QDs. These results suggest that a defect state can be purposely introduced to modify the electron-emission time of the QDs.

ACKNOWLEDGMENTS

The authors are grateful to Dr. J. Y. Chi and R. S. Hsiao for sample preparation and would like to thank the National Science Council of Taiwan for financially supporting this research under Contract No. NSC-97-2112-M-009-014-MY3. This work was partially supported by MOE ATU program.

[1]F. Heinrichsdorff, M. H. Mao, N. Kirstaedter, A. Krost, and D. Bimberg,

[This article is copyrighted as indicated in the article. Reuse of AIP content is subject to the terms at: http://scitation.aip.org/termsconditions. Downloaded to] IP: 140.113.38.11 On: Wed, 30 Apr 2014 15:26:01

Appl. Phys. Lett. **71**, 22 (1997).
[2]D. J. Eaglesham and M. Cerullo, Phys. Rev. Lett. **64**, 1943 (1990).
[3]D. Leonard, K. Pond, and P. M. Petroff, Phys. Rev. B **50**, 11687 (1994).
[4]J. M. Moison, F. Houzay, F. Barthe, and L. Leprince, Appl. Phys. Lett. **64**, 196 (1994).
[5]C. W. Snyder, J. F. Mansfield, and B. G. Orr, Phys. Rev. B **46**, 9551 (1992).
[6]H. Shoji, K. Mukai, N. Ohtsuka, M. Sugawara, T. Uchida, and H. Ishikawa, IEEE Photonics Technol. Lett. **7**, 1385 (1995).
[7]G. Yusa and H. Sakaki, Electron. Lett. **32**, 491 (1996).
[8]J. C. Campbell, D. L. Huffaker, H. Deng, and D. G. Deppe, Electron. Lett. **33**, 1337 (1997).
[9]C. M. A. Kapteyn, F. Heinrichsdorff, O. Stier, R. Heitz, M. Grundmann, and P. Werner, Phys. Rev. B **60**, 14265 (1999).
[10]R. J. Luyken, A. Lorke, A. O. Govorov, J. P. Kotthaus, G. Medeiros-Riberro, and P. M. Petroff, J. Appl. Phys. **74**, 2486 (1999).
[11]W. H. Chang, W. Y. Chen, M. C. Cheng, C. Y. Lai, T. M. Hsu, N. T. Yeh, and J. I. Chyi, Phys. Rev. B **64**, 125315 (2001).
[12]X. Letartre, D. Stievenard, and M. Lanoo, J. Appl. Phys. **69**, 7336 (1991).
[13]H. Drexler, D. Leonard, W. Hansen, J. P. Kotthaus, and P. M. Petroff, Phys. Rev. Lett. **73**, 2252 (1994).
[14]S. Sauvage, P. Boucaud, F. H. Julien, J.-M. Gerard, and J.-Y. Marzin, J. Appl. Phys. **82**, 3396 (1997).
[15]J. S. Wang, J. F. Chen, J. L. Huang, P. Y. Wang, and X. J. Guo, Appl. Phys. Lett. **77**, 3027 (2000).
[16]Y. Uchida, H. Kakibayashi, and S. Goto, J. Appl. Phys. **74**, 6720 (1993).
[17]J. F. Chen, R. S. Hsiao, C. K. Wang, J. S. Wang, and J. Y. Chi, J. Appl. Phys. **98**, 013716 (2005).
[18]R. Leon, Y. Kim, C. Jagadish, J. Zou, and D. J. H. Cockayne, Appl. Phys. Lett. **69**, 1888 (1996).
[19]A. O. Kosogov, P. Werner, U. Gosele, N. N. Ledentsov, D. Bimberg, V. M. Ustinov, A. Yu. Egorov, A. E. Zhukov, P. S. Kopev, N. A. Bert, and Zh. I. Alferov, Appl. Phys. Lett. **69**, 3072 (1996).
[20]S. Malik, C. Roberts, R. Murray, and M. Pate, Appl. Phys. Lett. **71**, 1987 (1997).
[21]S. J. Xu, X. C. Wang, S. J. Chua, C. H. Wang, W. J. Fan, J. Jiang, and X. G. Xie, Appl. Phys. Lett. **72**, 3335 (1998).
[22]S. S. Li and J. B. Xia, J. Appl. Phys. **84**, 3710 (1998).
[23]J. F. Chen, R. S. Hsiao, Y. P. Chen, J. S. Wang, and J. Y. Chi, Appl. Phys. Lett. **87**, 141911 (2005).
[24]J. F. Chen, R. S. Hsiao, S. H. Shih, P. Y. Wang, J. S. Wang, and J. Y. Chi, Jpn. J. Appl. Phys., Part 2 **43**, L1150 (2004).
[25]J. F. Chen, Y. Z. Wang, C. H. Chiang, R. S. Hsiao, Y. H. Wu, L. Chang, J. S. Wang, T. W. Chi, and J. Y. Chi, Nanotechnology **18**, 355401 (2007).
[26]P. N. Brunkov, A. Patane, A. Levin, L. Eaves, P. C. Main, Y. G. Musikhin, B. V. Volovik, A. E. Zhukov, V. M. Ustinov, and S. G. Konnikov, Phys. Rev. B **65**, 085326 (2002).
[27]O. Gunawan, H. S. Djie, and B. S. Ooi, Phys. Rev. B **71**, 205319 (2005).
[28]J. Ibanez, R. Leon, D. T. Vu, S. Chaparro, S. R. Johnson, C. Navarro, and Y. H. Zhang, Appl. Phys. Lett. **79**, 2013 (2001).
[29]J. F. Chen, R. S. Hsiao, M. F. Hsieh, J. S. Wang, and J. Y. Chi, J. Appl. Phys. **99**, 014303 (2006).
[30]J. F. Chen, R. S. Hsiao, W. D. Huang, Y. H. Wu, L. Chang, J. S. Wang, and J. Y. Chi, Appl. Phys. Lett. **88**, 233113 (2006).

[This article is copyrighted as indicated in the article. Reuse of AIP content is subject to the terms at: http://scitation.aip.org/termsconditions. Downloaded to] IP: 140.113.38.11 On: Wed, 30 Apr 2014 15:26:01